Investigation of a four-wave mixing signal generated in fiber-delivered CARS microscopy

Chang Su Jun,[1] Byoung Yoon Kim,[1] Ju Hyun Park,[2] Jae Yong Lee,[3] Eun Seong Lee,[3] and Dong-Il Yeom[4,*]

[1]Fiber Optics Laboratory, Department of Physics, Korea Advanced Institute of Science and Technology (KAIST), 373-1 Guseong-dong, Yuseong-gu, Daejeon 305-701, South Korea

[2]Nano and Bio Surface Science, University of Science and Technology (UST), 113 Gwahangno, Yuseong-gu, Daejeon 305-333, South Korea

[3]Nano-Bio Fusion Research Center, Korea Research Institute of Standards and Science (KRISS), 1 Doryong-dong, Yuseong-gu, Daejeon 305-340, South Korea

[4]Division of Energy Systems Research, Ajou University, San 5, Woncheon-dong, Yongtong-gu, Suwon 443-749, South Korea

*Corresponding author: diyeom@ajou.ac.kr

Received 29 March 2010; revised 10 June 2010; accepted 14 June 2010; posted 15 June 2010 (Doc. ID 126184); published 6 July 2010

We studied the nonlinear signal generated in the fiber at an anti-Stokes wavelength during the delivery of the picosecond (ps) pump and Stokes beams in coherent anti-Stokes Raman scattering (CARS) microscopy. A small non-phase-matched four-wave mixing (FWM) signal was prevalently observed in the fiber at the power level where other nonlinear processes, including self-phase modulation and cross-phase modulation, were well suppressed. We analyzed the features of the FWM signal generation by varying the location of temporal overlap between two input pulses in the fiber to compare this to the CARS signal generated in the sample. Numerical modeling based on the nonlinear Schrödinger equation was also conducted and clearly explains the results in the experiment. In addition, we experimentally verified the interferometric feature of this FWM signal with the CARS signal by employing a phase-shifting unit, which potentially suggests the use of the FWM signal as a local oscillator for the interferometric CARS system.

OCIS codes: 170.3880, 180.3170, 190.4370.

1. Introduction

Nonlinear optical microscopic technologies based on multiphoton absorption [1,2], higher harmonic generation [3,4], and coherent anti-Stokes Raman scattering (CARS) [5] are currently expanding their application areas by making good use of their unique properties in cell level imaging [6–8]. Particularly, CARS microscopes that employ two laser beams with a frequency difference corresponding to the Raman shift of a specific molecule in biological samples have received a great deal of attention due to their advantages, such as label-free chemical contrast, subwavelength spatial resolution in lateral directions, three-dimensional scanning, and high sensitivity. For future medical applications of CARS, it is desirable to implement the bioimaging, not through a microscope, but through an endoscope to observe tissue of an organism in real-time clinical diagnosis. While endoscopy has been successfully realized with conventional microscopes or other recent emerging technologies, including optical coherence tomography, two-photon emission fluorescence, and second harmonic generation, the CARS endoscope is still challenging at the *in vivo* level [6,9]. In the CARS

0003-6935/10/203916-06$15.00/0

endoscope, a fiber-based probe that efficiently transfers the pump and Stokes laser pulses and collects the anti-Stokes signal is a key element of the system. Previous studies have focused on the minimization of nonlinear distortion, such as self-phase modulation (SPM), cross-phase modulation (XPM), and Raman scattering, of two-color laser pulses during propagation along a fiber probe. In these studies, it has been found that the nonlinear spectral broadening can be well suppressed, even with a conventional single-mode fiber (SMF), at proper energy levels of picosecond (ps) pulse lasers. This enabled development of a prototype CARS endoscope using conventional SMFs [9].

In the present work, we observed and investigated the nonlinear signal generation at anti-Stokes wavelength via four-wave mixing (FWM) by two ps lasers in a fiber-delivered CARS microscope. We found that the non-phase-matched FWM signal is generated at a power level where other nonlinear effects, such as the SPM and XPM, are negligible. It should be noted that the FWM generation in the fiber-based probe has only very recently been reported [10]. In this study, they observed, for the first time, that the strong FWM signal is generated at an anti-Stokes wavelength during the fiber beam delivery of ps and synchronized femtosecond pulses and that it could severely disturb the CARS imaging in both conventional and large-mode-area (LMA) fibers. To avoid this frustrating factor, the researchers employed a novel design, including a dichroic mirror and another fiber for CARS signal detection, that enables efficient fiber-probe-based CARS imaging. In our work based on two ps beams, we carefully analyzed the origin of the FWM signal generation by adjusting the relative delay between two input pulses. We observed that the FWM signal is not appreciable in the case of the LMA fiber and could be suppressed in the normal SMF when the two pulses temporally overlap at the fiber midpoint. This behavior is expected to occur due to the overcoupling in the presence of walk-off along the fiber during non-phase-matched FWM signal generation; this is numerically confirmed by a simulation based on the generalized nonlinear Schrödinger equation [11]. The tendency of the FWM signal generated in the fiber with different time delays agrees well with the simulation results. In addition, we experimentally examined the interferometric feature of the generated FWM signal with the CARS signal in the sample by using a phase-shifting unit. Based on the result, possible alternative applications using this FWM signal as a local oscillator for the realization of an interferometric CARS system will be discussed.

2. Experimental Setup

We first carried out the experiment to analyze the FWM generation feature by varying the relative delays between pump and Stokes beams and comparing this with the CARS signal generated in the sample. Figure 1 illustrates the experimental setup used in

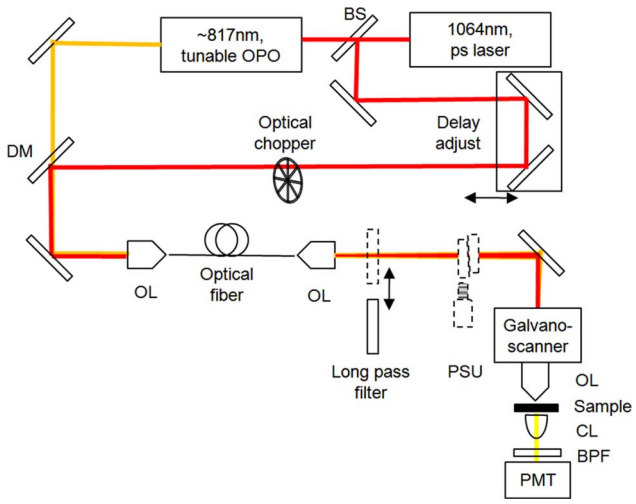

Fig. 1. (Color online) Experimental setup for the detection of both FWM and CARS signals. The long pass filter was used for blocking the FWM signal, and the phase-shifting unit (PSU) was employed to measure the interferometric CARS fringes. BS, beam splitter; DM, dichroic mirror; OL, objective lens; CL, condenser lens; BPF, bandpass filter; PMT, photomultiplier tube.

our work. A 1064 nm mode-locked Nd:YVO_4 laser (High-Q Laser GmbH) with a 7.3 ps pulse duration at a repetition rate of 76 MHz was used for a Stokes beam. An optical parametric oscillator (OPO) system (APE GmbH) synchronously pumped by the 1064 nm Stokes laser was employed for use as a tunable pump beam with a tuning range of 700–950 nm. The central wavelength of the pump beam was at 817 nm to excite the vibrational level ($\sim$2840 cm^{-1}) of the C—H stretching vibration of oil or polystyrene beads. The pump and Stokes beams were then combined spatially by a dichroic mirror. The temporal overlap was tuned by the adjustment of a delay line. Two spatially and temporally overlapped laser beams were coupled to the optical fiber by an objective lens (OL). The generated nonlinear signals were then monitored with a photomultiplier tube (PMT) after passing through the bandpass filter (BPF) centered at the anti-Stokes wavelength. We first measured the FWM signal generated from the fiber and the CARS signal at a fixed point of the sample. To distinguish the FWM and the CARS signals from the laser noise, an optical chopper was inserted in only the 1064 nm beam path. The peak-to-peak amplitude of the AC signal at the modulation frequency of the chopper was measured by an oscilloscope connected to the PMT. We observed that this AC signal was produced only when both the pump and the Stokes beams were combined, thus confirming the exclusion of the direct modulation signal of the Stokes beam from our measurement. An additional component of the phase-shifting unit was introduced to measure the interference, which is discussed in Subsection 3.C. In the experiment, the CARS image of the sample was acquired by a two-axis galvanoscanner and high-numerical-aperture (NA) OL (60×, water immersion, 1.2 NA). The CARS signal was collected by a condenser lens (CL) to deliver it to the PMT

through the BPF. The sample images were finally obtained from the digital-to-analog converter and related image processing through the computer.

3. Results and Discussions

A. FWM Generation in a Fiber-Delivered CARS Experiment

The FWM signal generation from the delivery fiber was experimentally examined for the normal SMF (HI780 Corning, HP780 Nufern) and the LMA photonic crystal fiber (PCF) (LMA20, NKT Photonics) with several fiber lengths. Based on the experimental method described in Section 2, we measured the intensity of the generated FWM signal as a function of relative delay variation between the Stokes and the pump beams in the absence of the sample. As described in Fig. 2(a), the temporal overlap between two pulses was tuned from the fiber front (delay A) to the fiber end (delay C) through the fiber midpoint (delay B) by adjustment of the delay line in the Stokes beam path. Before the measurement of the FWM signal, we checked the spectral properties of the pump and Stokes beams after fiber delivery and confirmed that there was not a significant spectral change of the laser beams due to the SPM or the XPM effect. We also expect that the pulse broadening effect could be almost negligible for a few-meters-long length of fiber propagation considering an estimated dispersion length of more than 300 m for our pulses. Figure 2(b) shows the FWM signal (squares) generated in the fiber with delays where the relative delay (x axis) is normalized by the pulse duration. The average power coupled to the normal SMF was measured to be 37 and 77 mW for the Stokes beam and the pump beam, respectively. The length of the fiber was first selected to be around 0.9 m, which corresponds to the walk-off length between the two input pulses. As shown in Fig. 2(b), we observed the two maxima of the FWM signal at the temporal overlap of A (fiber front) and C (fiber end) and the minimum at B (fiber middle). This "double-peak" tendency is more clearly seen when we use the 2.5 m length of the SMF, as shown in Fig. 2(b). We also measured the FWM signal for the LMA PCF with a length of 0.8 m, where the average power was similarly set to be 40 and 80 mW for the Stokes beam and the pump beam, respectively. We observed a relatively small FWM signal close to the noise level around delays A and C, as shown in Fig. 2(b). The measured FWM with a longer PCF results in tendencies similar to those of the shorter one (results not shown here).

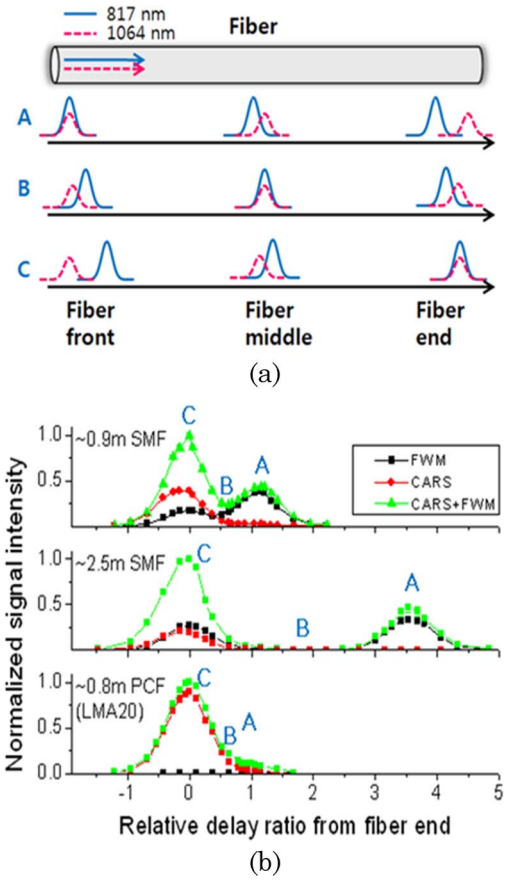

Fig. 2. (Color online) (a) Schematic representation of delay A, delay B, and delay C between the pump and the Stokes beams. (b) The characteristics of nonlinear signal generation in the experiment for the SMF and LMA PCF with different temporal overlaps (delays A, B, and C). Upper figure, normal SMF with a length of 0.9 m; middle figure, normal SMF with 2.5 m; lower figure, LMA PCF with 0.8 m. The locations of A, B, and C indicate the temporal overlap described in (a).

We then measured the CARS signal generated from an oil sample between two coverglasses to compare this with the FWM signal generated in the fibers. To isolate the FWM signal, we placed a long-pass filter after the fiber section, which effectively blocks the anti-Stokes wavelength. Although this method can be used to simply reject the FWM signal from the CARS measurement, it cannot be applied when one wants to implement CARS endoscopy in a single strand of the fiber, because the optical filter also obstructs the collection of the CARS signal through the fiber. The solid circles in Fig. 2(b) represent the CARS signal with different delays. The maximum signal appears only at delay C for both the SMF and the PCF, where the temporal overlap is matched at the fiber end (thus, also nearly matched at the sample). The triangles data show the combined signals with both the FWM and the CARS signal obtained by removing the long-pass filter. From the experimental results, the LMA PCF seems to be more appropriate as a delivery fiber for CARS imaging in terms of FWM signal suppression, which might be due to the relatively small nonlinearity for the core mode. However, it is interesting to note that the magnitude of the combined signal is different from the linear summation of each FWM and CARS signal at the SMF, indicating the interference between two signals. We first numerically analyze the FWM signal generated in the SMF with different delays in the next subsection, and a discussion of possible applications of the interferometric feature will follow.

B. Numerical Analysis of FWM Signal Generation in the SMF

The silica material exhibits large normal material dispersion at our operating wavelength range (600–1100 nm) and the contribution of the waveguide dispersion will not be significant for normal SMF and LMA PCF compared to a high-NA PCF possessing a very small core that tightly confines the propagating light. Thus, the FWM generation from the pump and Stokes beams will be a non-phase-matched process with very low conversion efficiency [11]. In addition, the nonlinear interaction in the fiber will occur at a limited fiber length due to the walk-off by large normal dispersion. Therefore, the FWM signal in these fibers could be negligible in most applications, such as wavelength conversion, but it showed comparable intensity with the CARS signal in the experiment, which initiates our numerical analysis.

In the numerical modeling based on the generalized nonlinear Schrödinger equation, we applied similar conditions used in the experiment. The 3 dB spectral bandwidths of the Stokes beam and the pump beam were set as 0.29 and 0.22 nm with peak powers of 218 W (average power, 77 mW) and 134 W (average power, 37 mW), respectively, where we assumed the transform-limited soliton pulse for both initial laser beams. The effective index area of the SMF (HI780) was set to 18.1 μm^2 with β_2 of 38.4 ps^2/km and β_3 of 0.015 ps^3/km at 817 nm, based on the effective index calculation of the core mode in the SMF by the finite-element method. The results are shown in Fig. 3(a). After propagation of the 0.9 m length of the SMF, new spectral components were observed at wavelengths of around 663 and 1552 nm while the pump (817 nm) and Stokes (1064 nm) beams nearly maintained their spectral shape. The generated signals were −65 dB less than the pump beam. To figure out the tendency observed in the experiment, we varied the relative delays between the pump and Stokes beams and monitored the power coupled to the anti-Stokes wavelength. In this numerical calculation, we modified the simulation conditions, due to the lack of computational capability, where the pump and Stokes wavelengths were set as 800 and 850 nm, respectively. We also introduced large normal dispersion (β_2 of 189.7 ps^2/km and β_3 of 1.091 ps^3/km at 817 nm) so that the pump and Stokes beams experienced complete walk-off after propagation of the fiber. Other parameters were set to the same values described in the original simulation above. We checked the results for several different conditions and found that the tendencies with delays are all similar to those described below. Figure 3(b) describes the power coupled to the anti-Stokes wave as a function of delays. The total power of the FWM signal was obtained from the integration of the spectral components around the anti-Stokes wavelength. As the temporal overlap was changed from fiber front (delay A) to fiber end (delay C), we could observe the "double-peak" tendency of the FWM signal that was similarly observed in the experiment. While the coupled power appears in symmetric fashion with delays in the simulation, the FWM signal observed in the experiment usually exhibits a smaller value at delay C than that at delay A, as shown in Fig. 2(b). We suspect that this comes from the polarization state mismatch between the two input beams during the propagation along the SMF in the experiment, which was not considered in the simulation.

To analyze "double peak" behavior in detail, we monitored the power at the anti-Stokes wavelength during propagation along the length of the fiber. Figure 3(c) shows the results for delays A, B, and C. When the pump beam temporally overlaps the Stokes beam at the fiber front (delay A), the generated FWM signal rapidly oscillates with large amplitude at the first stage. The oscillation could be interpreted as the repetition of the coupling and overcoupling processes between the generated FWM signal and the incident beams. The oscillating signal is then stabilized with a fixed value when the pump beam begins to temporally separate from the Stokes beam. In the case of delay C, the FWM signal gently increases along the fiber length without any oscillation. This feature was

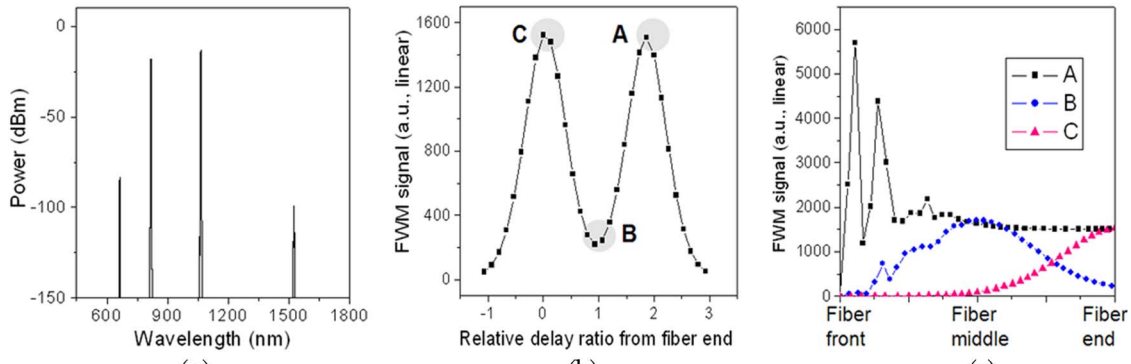

Fig. 3. (Color online) Numerical calculation of FWM generation in 0.9 m long SMF. (a) Spectral properties at the fiber end. (b) Calculated intensity around the anti-Stokes wavelength at the fiber end with different delays. (c) Changes of the FWM signal intensity along the fiber length for delays A, B, and C, which corresponds to the temporal overlaps of two pulses at the fiber front, middle, and end, respectively, as described in Fig. 2(a).

usually observed when the Stokes beam gradually approached the pump beam to temporally meet at the fiber end. More interestingly, the gently produced FWM signal was overcoupled to the pump and Stokes beams from the fiber midpoint in the case of delay B, resulting in a small FWM signal at the fiber output. This overcoupling and, thus, "double-peak," feature is commonly found at several different conditions with non-phase-matching in our simulation, which strongly supports our experimental observation. Further investigation for in-depth understanding of these phenomena is currently in progress.

C. Consideration of the Interferometric CARS Using the SMF

Although the FWM signal can be suppressed in the SMF around time delay B, the CARS signal will also be weakly generated due to the temporal overlap mismatch at the sample without subsequent delay compensation. Therefore, the FWM signal can be an annoying factor for the realization of fiber-based CARS microscopy, and can necessitate additional components for FWM signal blocking or an uncommon fiber with low nonlinearity. The triangle data in Fig. 2(b), however, implies the possibility of utilizing this FWM in a positive manner. As for the SMF in Fig. 2(b), the enhanced signal intensity (left peak) is larger than the summation of each of the FWM and CARS signals. The enhancement can be attributed to heterodyne amplification through nonlinear optical signal interference [12–15]. Because the FWM signal has the same frequency components as the sample CARS signal and it is coherent, it can act as a local oscillator that interferes with the CARS signal. Now we want to show the possibility of the interferometric CARS by setting up an interferometer and measuring interference fringes. Just by placing a phase-shifting unit that consists of two wedged BK7 glass blocks after the fiber section, as shown in Fig. 1, we could simply constitute an interferometer of two successively generated nonlinear optical signals [14,15]. By sliding one wedge against the other one, the overall glass thickness changes, and the relative phase between the CARS signal of the sample and the FWM signal from the fiber is accordingly varied.

Figure 4(a) clearly shows the interference fringes measured in this manner for the normal SMF delivery. The measured fringe period is consistent with the theoretical value 512 μm [15], which is calculated with the refractive indices of BK7 at 1064, 817, and 663 nm as 1.50664, 1.51042, and 1.51408, respectively. Since the modulation amplitude is proportional to the square root of the local oscillator intensity, we can amplify the CARS signal as we wish by increasing the pump and Stokes powers to the point before the sample begins to be damaged. Preliminary experiments of interferometric CARS images are carried out using a two-dimensional scanner setup. Figure 4(b) is an interferometric CARS image for 3 μm polystyrene beads embedded in cosmetic emulsion at the peak of the interference fringe shown in Fig. 4(a). The cosmetic

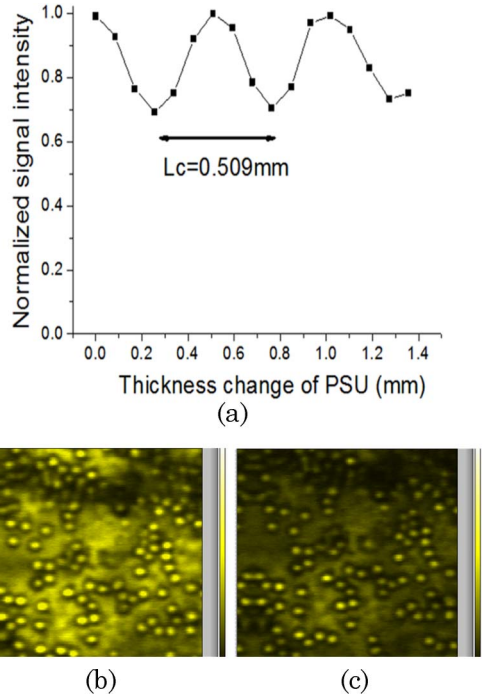

Fig. 4. (Color online) (a) Interference fringes measured from a fixed point of the sample in an interferometric CARS setup. (b) Interferometric CARS imaging of 3 μm polystyrene beads spread in cosmetic emulsion. (c) Pure CARS imaging of the same sample.

emulsion also has vibrational resonances around the Raman shift specified by the pump and Stokes beams, where its signal exhibits different CARS intensity and phase relative to polystyrene beads. The emulsion acts here as a strong background. The pure CARS image taken of the same sample with the FWM signal blocked is shown in Fig. 4(c). Comparing these figures, we can see the brighter image with slightly enhanced contrast in the interferometric CARS. This is because the image has been taken at the interference peak where only the CARS signals from the beads are in phase. The dark ring around each bead is caused by beam deflection that occurs at the interface of two different refractive indices. Although prominent improvement of the imaging quality is not seen due to the presently low intensity of the local oscillator, we expect further enhanced image quality by proper fiber selection.

4. Conclusion

In summary, we verified that FWM is quite prevalent in fiber-based CARS microscopy, as it was observed in most of the fibers, i.e., SMF, or even in LMA PCF, without any fiber-parameter restriction for phase-matching constraints. We analyzed the characteristics of the FWM signal by changing the temporal overlap of the pump and Stokes beams inside the fiber section and compared the experimental results with numerical simulations. While the non-phase-matched FWM background generally obstructs the CARS imaging of the sample, we suggest that this

FWM can be utilized as a reference signal of the interferometric CARS imaging application.

This study was supported by the Next-Generation New-Technology Development Program of MKE Korea, by the Bio-Signal Analysis Technology Innovation Program of the Ministry of Education, Science and Technology (MEST) Korea, and by a Korea Science and Engineering Foundation (KOSEF) grant funded by the Korean government (MEST) (grant 2010-0000628).

References

1. W. Denk, J. H. Strickler, and W. W. Webb, "Two-photon laser scanning fluorescence microscopy," Science **248**, 73–76 (1990).
2. S. W. Hell, K. Bahlmann, M. Schrader, A. Soini, H. M. Malak, I. Gryczynski, and J. R. Lakowicz, "Three-photon excitation in fluorescence microscopy," J. Biomed. Opt. **1**, 71–74 (1996).
3. R. Hellwarth and P. Christensen, "Nonlinear optical microscopic examination of structure in polycrystalline ZnSe," Opt. Commun. **12**, 318–322 (1974).
4. Y. Barad, H. Eisenberg, M. Horowitz, and Y. Silberberg, "Nonlinear scanning laser microscopy by third harmonic generation," Appl. Phys. Lett. **70**, 922–924 (1997).
5. M. D. Duncan, J. Reintjes, and T. J. Manuccia, "Scanning coherent anti-Stokes Raman microscope," Opt. Lett. **7**, 350–352 (1982).
6. L. Fu and M. Gu, "Fibre-optic nonlinear optical microscopy and endoscopy," J. Microsc. **226**, 195–206 (2007).
7. C. L. Evans and X. S. Xie, "Coherent anti-Stokes Raman scattering microscopy: chemical imaging for biology and medicine," Annu. Rev. Anal. Chem. **1**, 883–909 (2008).
8. H. W. Wang, I. M. Langohr, M. Sturek, and J. X. Cheng, "Imaging and quantitative analysis of atherosclerotic lesions by CARS-based multimodal nonlinear optical microscopy," Arterioscl. Thromb. Vasc. Biol. **29**, 1342–1342 (2009).
9. F. Légaré, C. L. Evans, F. Ganikhanov, and X. S. Xie, "Towards CARS endoscopy," Opt. Express **14**, 4427–4432 (2006).
10. M. Balu, G. Liu, Z. Chen, B. J. Tromberg, and E. O. Potma, "Fiber delivered probe for efficient CARS imaging of tissues," Opt. Express **18**, 2380–2388 (2010).
11. G. P. Agrawal, *Nonlinear Fiber Optics*, 4th ed. (Academic, 2007).
12. E. S. Lee and J. W. Hahn, "Relative phase control between two successive coherent anti-Stokes Raman-scattering signals for the recovery of spectral lines," Appl. Opt. **33**, 8302–8305 (1994).
13. E. R. Andresen, S. R. Keiding, and E. O. Potma, "Picosecond anti-Stokes generation in a photonic-crystal fiber for interferometric CARS microscopy," Opt. Express **14**, 7246–7251 (2006).
14. J. Y. Lee, E. S. Lee, and Y. S. Yoo, "Novel equipment setup simplifies nonlinear interferometric microscopy," SPIE Newsroom, doi: 10.1117/2.1200609.0411 (2006) .
15. E. S. Lee, J. Y. Lee, and Y. S. Yoo, "Nonlinear optical interference of two successive coherent anti-Stokes Raman scattering signals for biological imaging applications," J. Biomed. Opt. **12**, 024010 (2007).